

*Observed Correlations Between Multi-Decadal Sea Surface Temperature  
Variability and ITCZ Migrations*

*Authors*

Brian Green\*<sup>1</sup>

John Marshall<sup>1</sup>

Aaron Donohoe<sup>2</sup>

*Affiliations*

1: Department of Earth, Atmospheric, and Planetary Sciences, Massachusetts Institute of  
Technology, Cambridge, Massachusetts 02139, USA

2: Applied Physics Laboratory, University of Washington, Seattle, Washington 98105,  
USA

*Contact Information for the Corresponding Author*

Brian Green

Department of Earth, Atmospheric, and Planetary Sciences, Massachusetts Institute of  
Technology

77 Massachusetts Ave, Bldg 54-1519

Cambridge, MA 02142

brianmg@mit.edu

### *Introduction Paragraph*

The Inter-Tropical Convergence Zone (ITCZ) is a global-scale band of tropical precipitation lying, in the annual mean, just north of the equator. Its location in the Northern Hemisphere can be connected to the atmosphere's hemispheric energy balance: the atmosphere in the Northern Hemisphere is heated more strongly than in the Southern Hemisphere, creating an inter-hemispheric temperature contrast. Offsetting the heating imbalance, the atmospheric circulation and associated ITCZ are biased north of the equator, accomplishing a southwards cross-equatorial energy transport (1-3). This relationship between inter-hemispheric temperature contrasts and the position of the ITCZ is robust over the seasonal cycle (4), in inter-annual variability (5), in proxy paleo data (6), and in a range of modeling studies in response to external forcing (7-12). In this study, we seek observed connections between the position of the ITCZ and indices of multi-decadal sea surface temperature variability over the 20<sup>th</sup> Century. We find that during periods when the North Atlantic and North Pacific oceans are anomalously warm, the Northern Hemisphere's troposphere is warmer than the Southern Hemisphere's, and the ITCZ and atmospheric circulation are shifted further to the north. Our results suggest an important role for the ocean circulation in modulating ITCZ migrations on decade- and-longer timescales, and that decadal predictions of the circulation can be leveraged to inform decadal predictions of precipitation in the tropical belt.

### *Extratropical SSTs, Cross-Equatorial Energy Transport and the ITCZ Position*

The ITCZ occupies a narrow range of latitudes, particularly in the Atlantic and eastern Pacific oceans. It is located between the atmosphere's two Hadley cells, which are

responsible for the majority of the atmosphere's meridional energy transport in the tropics (1), and migrates with these circulations over the course of the seasonal cycle (4). When the sun heats the Northern Hemisphere (NH) atmosphere more strongly during boreal summer, the Hadley cells are centered north of the equator, as is the ITCZ, and they transport energy southwards across the equator, opposing the solar heating imbalance. The opposite occurs during boreal winter, when the Hadley cells and the ITCZ are centered in the Southern Hemisphere (SH).

Extratropical temperature contrasts between the hemispheres, shifts in the Hadley cells, and accompanying displacements of the ITCZ have received much recent attention in modeling studies (7-12), and a framework has emerged for interpreting their connection (11). When the ocean, or a top-of-atmosphere radiative imbalance, preferentially heats one hemisphere's extratropical atmosphere relative to the other, eddies diverge a fraction of that energy into the tropics, and the remainder is radiated away to space or stored in the climate system. The Hadley cells, and thus the ITCZ, shift into the heated hemisphere and transport that energy across the equator into the cooler hemisphere. This behavior has been seen in climate models simulating a range of energetic forcings, including changes in high-latitude ice cover (8), changes in the Atlantic Meridional Overturning Circulation's (AMOC) meridional energy transport (7, 9), and global warming (12). Across these simulations, changes in the sea surface temperature (SST) contrast between the NH and SH are correlated with meridional shifts in the Hadley cells and migrations of the ITCZ.

These ideas are also relevant for understanding the modern climatology. Northwards cross-equatorial energy transport by the AMOC heats the atmosphere in the

NH through surface energy fluxes, cooling it in the SH. This leads, it has been argued, to the climatological, annual-mean position of the ITCZ residing north of the equator (1,2). Similar to boreal summer, the atmosphere again responds to the energy imbalance by shifting the Hadley cells northwards, transporting a fraction of the energy input into the NH back southwards across the equator, helping to equilibrate the energy budget.

### *SST, Precipitation, and Tropospheric Co-Variability Over the 20<sup>th</sup> Century*

Motivated by the surface temperature-ITCZ connections seen in climate models and their associated energetic framework, here we turn to the observational record to investigate those connections over the 20<sup>th</sup> Century. We use the Smith et al (2012; 13) global precipitation reconstruction (at 5°x5° resolution from 1900-2008) to analyze variations in precipitation. Estimates of the time and zonal-mean precipitation climatology are shown in Figure 1a, b. The ITCZ is clearly seen in the tropical Atlantic and Pacific, and zonal-mean tropical rainfall peaks north of the equator. Defining the position of the ITCZ as the centroid of the zonal-mean precipitation between 20°N and 20°S (4), the time series of its anomaly about a mean latitude of 1.7°N is shown in Figure 1e. We see that there is considerable interannual variability, but that post 1930 the ITCZ was slightly further north than its long-term position, whereas in the early part of the 20<sup>th</sup> Century it was somewhat more southward. Using a low-pass filter with a cutoff period of 10 years to isolate the low frequency variability, we see from Figure 2a that, when regressed against a northwards shift in the ITCZ position, precipitation anomalies peak in the western tropical Pacific, with a smaller north-south dipole in the tropical Atlantic. In the zonal mean (see Fig. 2b), a dipole of precipitation anomalies straddles the mean ITCZ position,

reflecting a northwards shift of the tropical precipitation centroid. Are these decadal migrations in the ITCZ associated with extratropical SST variability?

Two leading modes of extratropical NH SST variability are the Atlantic Multi-decadal Oscillation (AMO; 14) and the Pacific Decadal Oscillation (PDO; 15); these modes have been linked to variability in tropical precipitation (16) and cloudiness (17) in their respective basins. Using the HadISST reconstruction from 1870-2012 (18), the AMO index is defined as the difference between average North Atlantic and global-mean SST (19). The PDO index is similarly defined here as the global-mean SST subtracted from its average value in the North Pacific. The SST anomalies associated with  $1\sigma$  warm anomalies of the annual-mean AMO (+0.14K) and PDO (+0.12K) indices peak in the NH extratropics (Figure 1c, d), with a basin-wide warm anomaly in the North Atlantic and a warm-cold zonal dipole in the Pacific, respectively. As shown in Figure 1f and g, the AMO and PDO indices show variability at a range of timescales from yearly to multi-decadal, and appear correlated with the decadal ITCZ variability seen in Figure 1g: a warm-phase (positive anomaly) AMO with a northwards ITCZ anomaly in the 1930's, and a warm-cold PDO transition with a southwards ITCZ shift around 1980.

To quantitatively test these connections, we perform a multiple regression analysis on the ITCZ position using the AMO and PDO as predictors, low-pass filtering each time series to isolate its decadal variability (see the Methods section for details). We find the ITCZ shifts north when the North Atlantic and Pacific are warm: a  $1\sigma$  AMO anomaly is associated with a northwards ITCZ shift of  $0.07^\circ \pm 0.05^\circ$  (a  $1\sigma$  error estimate), and a  $1\sigma$  PDO anomaly is associated with a northwards ITCZ shift of  $0.10^\circ \pm 0.06^\circ$ , shown in Table 1. The AMO and PDO indices explain, respectively, 11% and 14%

of the ITCZ variance at these timescales, and their combined regression explains 25% of the variance, which is also significant to  $1\sigma$ . It should be noted that the AMO and PDO are not correlated with one another. Moreover, the ITCZ position is not correlated with the El Niño-Southern Oscillation (ENSO) and its Niño-3 index ( $r = 0.02$ ).

Local precipitation anomalies, when multiple-regressed against the AMO and PDO, also show patterns indicative of meridional ITCZ shifts. Maps of precipitation anomalies associated with warm phase AMO and PDO indices have significant (to  $1\sigma$ ) spatial correlations with those associated with a northwards ITCZ shift (Figure 2c, e) – between  $20^\circ\text{N}$  and  $20^\circ\text{S}$ ,  $r_{\text{AMO,ITCZ}} = 0.65$  and  $r_{\text{PDO,ITCZ}} = 0.54$ . Precipitation anomalies associated with a warm phase AMO show a similar tripole pattern in the western Pacific as those associated with a northwards ITCZ shift, and positive anomalies are also seen in the northern tropical Atlantic and the Sahel, consistent with Zhang and Delworth (2006; 16). The pattern of anomalies associated with a warm phase PDO show a slightly different pattern, with a north-south dipole stretching across the Pacific. North-south dipoles of precipitation anomalies, centered on the time-mean ITCZ position, are seen more clearly when zonal-mean precipitation anomalies are multiple-regressed against the AMO and PDO indices (Figure 2d, f). These patterns are consistent with a northwards shift of the tropical precipitation centroid, also pointing to a northwards shift of the ITCZ when the North Atlantic and Pacific oceans are anomalously warm.

Consistent with a northwards ITCZ shift, we observe correlations between anomalies in the Hadley cells, inter-hemispheric tropospheric temperatures, and the AMO and PDO indices. Figure 3 shows patterns of atmospheric overturning circulation and inter-hemispheric tropospheric temperature anomalies from the NCEP/NCAR reanalysis

(20) multiple-regressed against the AMO and the PDO indices. During warm phases of the AMO and PDO, anomalous cross-equatorial Hadley cells are seen (Figure 3a,b) with rising motion north of the equator. We also observe anomalous inter-hemispheric tropospheric temperature contrasts reflecting a relatively warm NH troposphere (Figure 3c,d). Hemispherically asymmetric temperature anomalies associated with a warm North Atlantic are spread over the depth of the troposphere with a local maximum of 0.15K near the surface (at 850hPa), while those associated with a warm North Pacific peak in the mid-troposphere (at 700hPa) with a weaker magnitude of 0.10K. Conversely, overturning streamfunction anomalies are larger when the North Pacific is warm – the 7.4Sv maximum anomaly in Figure 3b is larger than the 4.8Sv maximum anomaly in Figure 3a associated with a warm North Atlantic. These stronger streamfunction anomalies associated with a warm-phase PDO are consistent with its greater ITCZ shift, but not with the stronger inter-hemispheric temperature contrast anomalies associated with a warm-phase AMO.

To further test the relationships between tropospheric variability and the AMO and PDO, we define indices of the Hadley cell strength at the equator ( $\Psi_{eq}$ ) and the inter-hemispheric temperature contrast in the troposphere ( $T_{interhem}$ ) (see the Methods section for details). Multiple-regressing these indices against the AMO and PDO, we find that the AMO explains more of their variance than the PDO (Table 1). At decadal timescales, the AMO index is, to  $2\sigma$ , significantly correlated with both inter-hemispheric temperature contrasts and cross-equatorial mass transport by the Hadley cells. The stronger streamfunction anomalies associated with the PDO in Figure 3b are now seen to be the result of a larger regression slope between the PDO and  $\Psi_{eq}$ , a slope that is not

significantly different than it is for the AMO. It is remarkable to note that the AMO index explains over 70% of the low-pass filtered inter-hemispheric tropospheric temperature contrast in the reanalysis. While the PDO is correlated with Hadley cell shifts, it is not correlated with  $T_{\text{interhem}}$ , which suggests different mechanisms for the PDO and AMO in modulating ITCZ migrations.

### *Discussion of Timescales and Mechanisms*

Our observed connections between a warm North Atlantic, northwards ITCZ and Hadley cell shifts, and inter-hemispheric tropospheric temperature contrasts are all consistent with the framework proposed in Kang et al (2009), where the ocean forces the atmosphere through surface energy fluxes. The relationship between North Atlantic SST and surface energy fluxes, however, is a function of timescale: on decade-and-longer timescales, warm SST anomalies are correlated with an upward flux of energy to the atmosphere, while on inter-annual timescales the correlation is reversed and the atmosphere forces SST anomalies (21). Additionally, the pattern of SST anomalies associated with a high-pass filtered AMO index (10 year cutoff period) is very similar to that associated with the negative phase of the North Atlantic Oscillation index (NAO; 22; Supplementary Material Figure 1), a measure of internal atmospheric variability (23). Between 1870 and 2012, the high-pass filtered AMO index and yearly NAO index have a correlation coefficient of -0.34, indicating that inter-annual variability in the AMO index is affected by the atmospheric circulation variability characterized by the NAO. Thus, at high frequencies, the AMO is a consequence of that atmospheric variability being damped by the ocean, instead of the ocean circulation (via SSTs) forcing the atmospheric

circulation. Therefore, we do not expect the Kang et al (2009) framework connecting extratropical SST anomalies and the ITCZ position to apply to the high frequency AMO variability. Regressions using high-pass filtered time series confirms this: the high-pass filtered AMO index explains, respectively, 4%, 1%, and 24% of the ITCZ position,  $\Psi_{eq}$ , and  $T_{interhem}$  variance, much less than the low-pass filtered values in Table 1.

On decadal timescales, though, the observed correlations between a warm North Atlantic and upward turbulent fluxes of energy from the surface ocean to the atmosphere above (21) are consistent with the mechanism for forced northwards ITCZ shifts proposed in Kang et al (2009). As such, correlations at these timescales between the AMO index and the ITCZ position, Hadley cell anomalies, and inter-hemispheric tropospheric temperature contrasts further suggest that variations in the ocean's energy transport have driven decadal SST variability in the North Atlantic over the 20<sup>th</sup> Century. Such connections can break down if, for example, aerosols – see Booth et al (2012; 24) and a critical analysis by Zhang et al (2013; 25) – or stochastic mixed-layer dynamics (26) usurp the ocean circulation's role in AMO variability. However, both of those mechanisms rely on a zero or negative correlation between SST anomalies and upward surface energy fluxes, correlations which on decadal timescales have been observed to be positive over the 20<sup>th</sup> Century.

The mechanisms connecting North Pacific SSTs to the ITCZ position and Hadley cell anomalies are likely different than in the North Atlantic. The Pacific Ocean transports less energy across the equator than the Atlantic (27), and its energy transport is thought to be dominated by shallow wind-driven circulations rather than a deep overturning circulation like the AMOC (28). Decadal SST variability in the North Pacific

may be forced by, for example, ENSO, ocean circulation variability, and extratropical atmospheric variability (29), making PDO-ITCZ connections likely the result of a combination of processes. Because the temperature anomalies in Figure 3d associated with the PDO are weaker and not surface-intensified like they are with the AMO, the extratropical Pacific ocean is likely not heating the atmosphere via a cross-equatorial energy transport. Additionally, as mentioned above, ENSO is only weakly correlated with the ITCZ position, and its associated inter-hemispheric temperature contrast and Hadley cell anomalies are about half as strong per standard deviation as they are for PDO anomalies in Figure 3 (not shown). This suggests that ENSO is not directly playing a key role in zonal-mean ITCZ dynamics. Tropical forcing of North Pacific SSTs does contribute to PDO index anomalies, though, and 300hPa height anomalies show a distinctive wave train pattern originating in the tropics when regressed against the PDO (Supplementary Material Figure 2). So, even though ENSO does not appear to directly influence the ITCZ position, it could have an indirect influence through teleconnections to the extratropical atmosphere.

In conclusion we have shown that 25% of the variance of decadal ITCZ variability is associated with extratropical SST variability, with the AMO and PDO making roughly equal contributions. In particular, despite being confined to the smaller Atlantic basin, the AMO explains 40% of the Hadley cell variability at the equator and a remarkable 75% of the interhemispheric tropospheric temperature variability. It is widely believed that on decadal timescales the AMO is affected by variations in the strength of the AMOC (see the review by Buckley and Marshall, 2016; 30), the primary mode of climate and climate variability that connects the two hemispheres together. Moreover, the

AMOC has predictability on decadal timescales (31) and its cross-equatorial energy transport are responsible, we believe, for the observed co-variability of SST and surface heat flux anomalies in the Atlantic sector. Our study suggests that AMOC predictability could be leveraged for predictability of ITCZ migrations with implications for precipitation along the entire tropical belt.

## *Methods*

To define the AMO and PDO indices, we respectively area-weight SST from 80°W-0° longitude and 0°-60°N latitude, and 110°E-100°W longitude and 20°N-70°N latitude. The indices' values are then defined as the global-mean SST subtracts from these area-weighted values.

All of the regressions performed in the figures and table use the AMO and PDO indices as predictors in a multiple regression analysis. All three time series (the AMO, PDO, and the predictand) are first low-pass filtered, then de-trended prior to the regression. The low-pass filter is an order-10 Butterworth filter with a cutoff period of 10 years. Both un-filtered yearly anomalies of the AMO and PDO indices, and the low-pass filtered time series are nearly uncorrelated:  $r_{AMO,PDO} = -0.10$  and  $-0.05$ , respectively.

Because the resulting filtered time series no longer resemble AR-1 processes, the effective degrees of freedom in the regressions for error estimation are then calculated following Bretherton et al (1999; 32) eq. 30, summing over the first 20 1-year lags. The significance of spatial correlations between the precipitation anomaly maps in Figure 2 is estimated by calculating the effective number of spatial degrees of freedom in the low-pass filtered precipitation anomalies following Bretherton et al (1999) eq. 3.

The indices  $\Psi_{eq}$  and  $T_{interhem}$  are respectively calculated from annual-mean values of the meridional overturning streamfunction and zonal-mean temperatures in the NCEP/NCAR reanalysis between 1948 and 2012. Their time series are then low-pass filtered and detrended before being multiple-regressed against the AMO and PDO indices to obtain the values in Table 1.  $\Psi_{eq}$  is the time series of the vertical-mean streamfunction

evaluated at the equator. This is calculated from zonal-mean meridional velocities which are first corrected to remove any vertical-mean meridional mass transport across a latitude circle. Hemisphere-mean temperatures in the troposphere are calculated by averaging zonal-mean temperature over latitude and between the surface and 300hPa. The difference between the Northern and Southern Hemisphere's values defines the  $T_{\text{interhem}}$  index where positive values indicate a warmer Northern Hemisphere troposphere.

In Figure 3, the temperature anomaly at a given latitude  $y$  can be split into symmetric and asymmetric components:  $T(y) = T_{\text{asym}}(y) + T_{\text{sym}}(y)$ , with  $T_{\text{asym}}(y) = -T_{\text{asym}}(-y)$  and  $T_{\text{sym}}(y) = T_{\text{sym}}(-y)$ .

## References

1. Marshall, J., Donohoe, A., Ferreira, D., & McGee, D. The ocean's role in setting the mean position of the Inter-Tropical Convergence Zone. *Climate Dynamics* **42.7-8**, 1967-1979 (2014).
2. Frierson, D. M. W., et al. Contribution of ocean overturning circulation to tropical rainfall peak in the Northern Hemisphere. *Nature Geoscience* **6.11**, 940-944 (2013).
3. Schneider, T., Bischoff T., & Haug, G. H. Migrations and dynamics of the intertropical convergence zone. *Nature* **513.7516**, 45-53 (2014).
4. Donohoe, A., Marshall, J., Ferreira, D., & McGee, D. The relationship between ITCZ location and cross-equatorial atmospheric heat transport: From the seasonal cycle to the Last Glacial Maximum. *Journal of Climate* **26.11**, 3597-3618 (2013).
5. Donohoe, A., Marshall, J., Ferreira, D., Armour, K., & McGee, D. The interannual variability of tropical precipitation and interhemispheric energy transport. *Journal of Climate* **27.9**, 3377-3392 (2014).
6. McGee, D., Donohoe, A., Marshall, J., & Ferreira, D. Changes in ITCZ location and cross-equatorial heat transport at the Last Glacial Maximum, Heinrich Stadial 1, and the mid-Holocene. *Earth and Planetary Science Letters* **390**, 69-79 (2014).

7. Zhang, R., & Delworth, T. L. Simulated tropical response to a substantial weakening of the Atlantic thermohaline circulation. *Journal of Climate* **18.12**, 1853-1860 (2005).
8. Chiang, J. C. H., & Bitz, C. M. Influence of high latitude ice cover on the marine Intertropical Convergence Zone. *Climate Dynamics* **25.5**, 477-496 (2005).
9. Broccoli, A. J., Dahl, K. A., & Stouffer, R. J. Response of the ITCZ to Northern Hemisphere cooling. *Geophysical Research Letters* **33.1** (2006).
10. Kang, S. M., Held, I. M., Frierson, D. M. W., & Zhao, M. The response of the ITCZ to extratropical thermal forcing: Idealized slab-ocean experiments with a GCM. *Journal of Climate* **21.14**, 3521-3532 (2008).
11. Kang, S. M., Frierson, D. M. W., & Held, I. M. The tropical response to extratropical thermal forcing in an idealized GCM: The importance of radiative feedbacks and convective parameterization. *Journal of the Atmospheric Sciences* **66.9**, 2812-2827 (2009).
12. Frierson, D. M. W., & Hwang, Y. T. Extratropical influence on ITCZ shifts in slab ocean simulations of global warming. *Journal of Climate* **25.2**, 720-733 (2012).

13. Smith, T. M., Arkin, P. A., Ren, L., & Shen, S. S. P. Improved reconstruction of global precipitation since 1900. *Journal of Atmospheric and Oceanic Technology* **29.10**, 1505-1517 (2012).
14. Kerr, R. A. A North Atlantic climate pacemaker for the centuries. *Science* **288.5473**, 1984-1985 (2000).
15. Mantua, N. J., Hare, S. R., Zhang, Y., Wallace, J. M., & Francis, R. C. A Pacific interdecadal climate oscillation with impacts on salmon production. *Bulletin of the American Meteorological Society* **78.6**, 1069-1079 (1997).
16. Zhang, R., & Delworth, T. L. Impact of Atlantic multidecadal oscillations on India/Sahel rainfall and Atlantic hurricanes. *Geophysical Research Letters* **33.17** (2006).
17. Deser, C., Phillips, A. S., & Hurrell, J. W. Pacific interdecadal climate variability: Linkages between the tropics and the North Pacific during boreal winter since 1900. *Journal of Climate* **17.16**, 3109-3124 (2004).
18. Rayner, N. A., et al. Global analyses of sea surface temperature, sea ice, and night marine air temperature since the late nineteenth century. *Journal of Geophysical Research: Atmospheres (1984–2012)* **108.D14** (2003).

19. Trenberth, K. E., and Shea, D. J. Atlantic hurricanes and natural variability in 2005. *Geophysical Research Letters* **33.12** (2006).
20. Kalnay, Eugenia, et al. The NCEP/NCAR 40-year reanalysis project. *Bulletin of the American Meteorological Society* **77.3**, 437-471 (1996).
21. Gulev, S. K., Latif, M., Keenlyside, N., Park, W., & Koltermann, K. North Atlantic Ocean control on surface heat flux on multidecadal timescales. *Nature* **499.7459**, 464-467 (2013).
22. Hurrell, J. W. Decadal trends in the North Atlantic Oscillation: regional temperatures and precipitation. *Science* **269.5224**, 676-679 (1995).
23. Marshall, J., et al. North Atlantic climate variability: phenomena, impacts and mechanisms. *International Journal of Climatology* **21.15**, 1863-1898 (2001).
24. Booth, B. B. B., Dunstone, N. J., Halloran, P. R., Andrews, T., & Bellouin, N. Aerosols implicated as a prime driver of twentieth-century North Atlantic climate variability. *Nature* **484.7393**, 228-232 (2012).
25. Zhang, R., et al. Have aerosols caused the observed Atlantic multidecadal variability? *Journal of the Atmospheric Sciences* **70.4**, 1135-1144 (2013).

26. Clement, A., et al. The Atlantic Multidecadal Oscillation without a role for ocean circulation. *Science* **350.6258**, 320-324 (2015).
27. Trenberth, K. E., & Caron, J. M. Estimates of meridional atmosphere and ocean heat transports. *Journal of Climate* **14.16**, 3433-3443 (2001).
28. Ferrari, R., & Ferreira, D. What processes drive the ocean heat transport? *Ocean Modelling* **38.3**, 171-186 (2011).
29. Schneider, N., & Cornuelle, B. D. The Forcing of the Pacific Decadal Oscillation\*. *Journal of Climate* **18.21**, 4355-4373 (2005).
30. Buckley, M., & Marshall, J. (2016). Accepted for publication in *Reviews of Geophysics*.
31. Tulloch, R., & Marshall, J. Exploring mechanisms of variability and predictability of Atlantic meridional overturning circulation in two coupled climate models. *Journal of Climate* **25.12**, 4067-4080 (2012).
32. Bretherton, C. S., Widmann, M., Dymnikov, V. P., Wallace, J. M., & Blade, I. The effective number of spatial degrees of freedom of a time-varying field. *Journal of Climate* **12.7**, 1990-2009 (1999).

### *Acknowledgements*

This study was supported by NASA and NOAA.

### *Author Contributions*

B.G., J.M., and A.D. conceived and designed the analysis. B.G. performed the analysis.

B.G, J.M., and A.D. co-wrote the paper.

## Figure Captions

*Figure 1.* Precipitation climatology, and North Atlantic and North Pacific SST variability. Top: annual mean precipitation (a; contour interval: 1mm/day) and its zonal average (b) from the Smith et al (2012) reconstruction. The green dashed line indicates the time-mean ITCZ position of 1.7°N. Middle: SST anomalies regressed against +1 $\sigma$  of the annual-mean AMO (c) and PDO (d) indices. The contour interval is 0.1K. Black lines indicate the regions SST is averaged over to generate the AMO and PDO indices. Bottom: time series of ITCZ position (e), AMO index (f), and PDO index (g) anomalies.

*Figure 2.* Maps of precipitation anomalies. Local precipitation anomalies (a, c, e) and their zonal averages (b, d, f) regressed against + $\sigma/2$  ITCZ shift (a, b), a +1 $\sigma$  AMO index (+0.14K; c, d), and a +1 $\sigma$  PDO index (+0.12K; e, f). Light and dark grey contours are respectively the 3mm/day and 6mm/day climatology of annual mean precipitation. Green shadings around the zonal-mean anomalies are  $\pm 1\sigma$  error estimates, and the green dashed line indicates the time-mean ITCZ position of 1.7°N.

*Table 1.* Fraction of the variance explained by the AMO and PDO indices for the ITCZ position, equatorial streamfunction anomaly  $\Psi_{\text{eq}}$ , and tropospheric inter-hemispheric temperature contrast anomaly  $T_{\text{interhem}}$  from the NCEP/NCAR reanalysis. Anomalies are for +1 $\sigma$  of the AMO (0.14K) and PDO (0.12K), and error estimates are  $\pm 1\sigma$ .

*Figure 3.* Atmospheric circulation anomalies. Top: meridional mass transport streamfunction anomalies from the NCEP/NCAR reanalysis from 1948-2012 regressed against +0.14K AMO and +0.12K PDO anomalies (a, b respectively). Blue contours indicate negative anomalies and counter-clockwise rotation, indicated by chevrons, and red contours indicate positive anomalies and clockwise rotation. The contour interval is 1Sv ( $10^9$  kg/s), and the zero contour is not shown. Bottom: the hemispherically asymmetric component of zonal-mean temperature anomalies regressed against +0.14K AMO and +0.12K PDO anomalies (c, d respectively). At a given latitude  $y$ , the temperature anomaly can be split into symmetric and asymmetric components:  $T(y) = T_{asym}(y) + T_{sym}(y)$ , with  $T_{asym}(y) = -T_{asym}(-y)$  and  $T_{sym}(y) = T_{sym}(-y)$ . Contour interval: 0.025K.

*Supplementary Figure 1.* North Atlantic SST variability. SST anomalies regressed against  $-1\sigma$  of the NAO index (a), and +0.14K anomalies of the high-pass and low-pass filtered AMO index (b, c). Yearly-mean values are used in the regressions, the high- and low-pass filters use cutoff periods of 10 years, and the filters are applied to both the SST anomalies and the AMO index prior to the regression. Contour interval: 0.05K.

*Supplementary Figure 2.* Height anomalies associated with the PDO. Low-pass filtered geopotential height anomalies at 300hPa associated with a  $+1\sigma$  (0.14K) anomaly of the low-pass filtered AMO index (a) and a  $+1\sigma$  (0.12K) PDO anomaly (b). Solid contours indicate positive anomalies, and dashed contours negative anomalies. The contour interval is 2m.

Figure 1

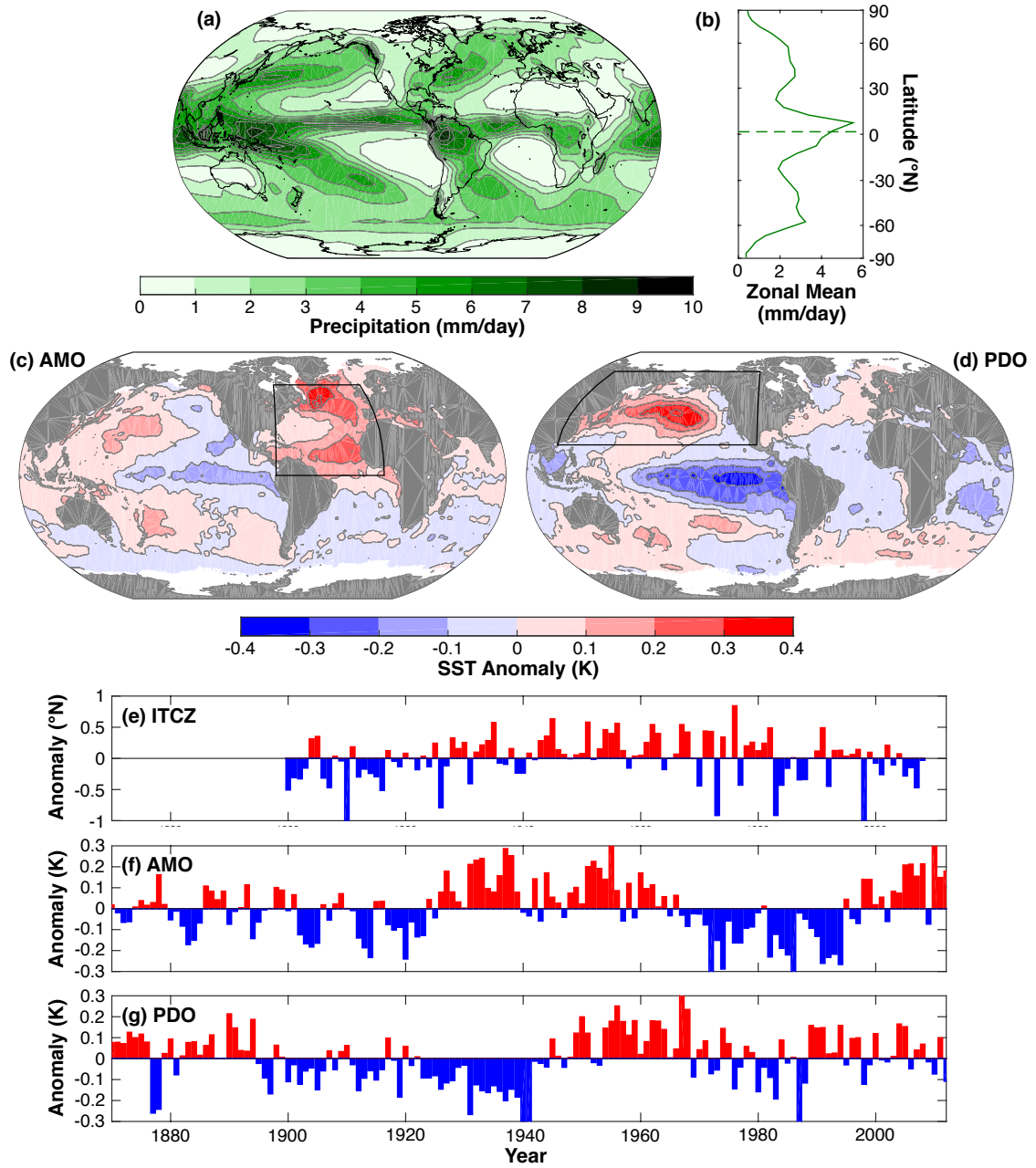


Figure 2

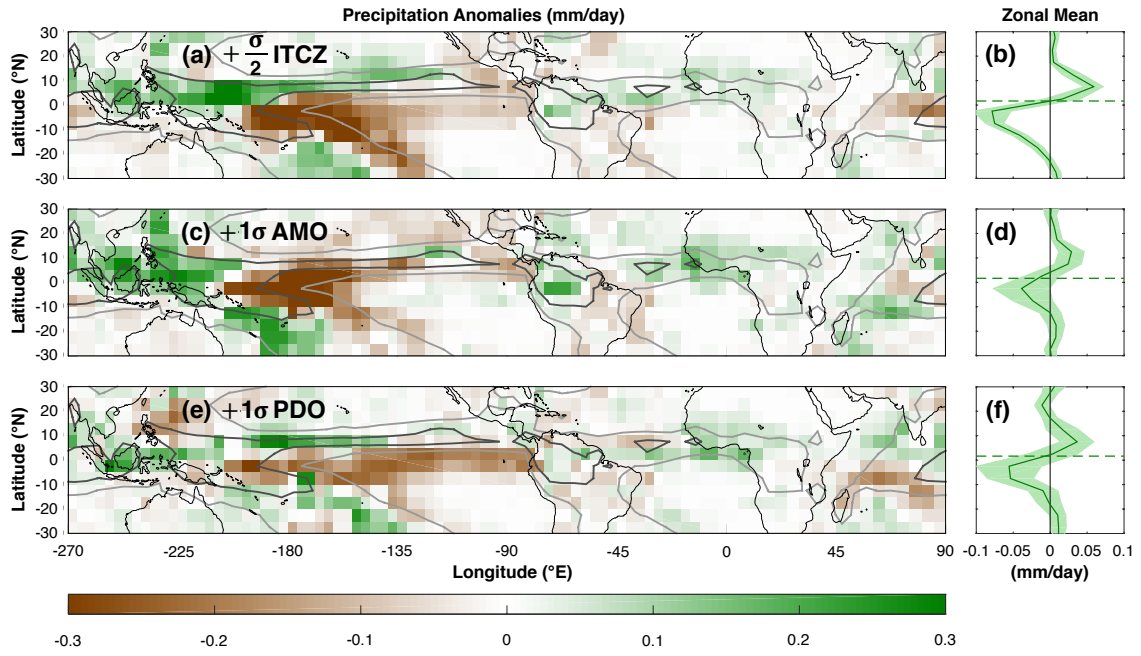


Figure 3

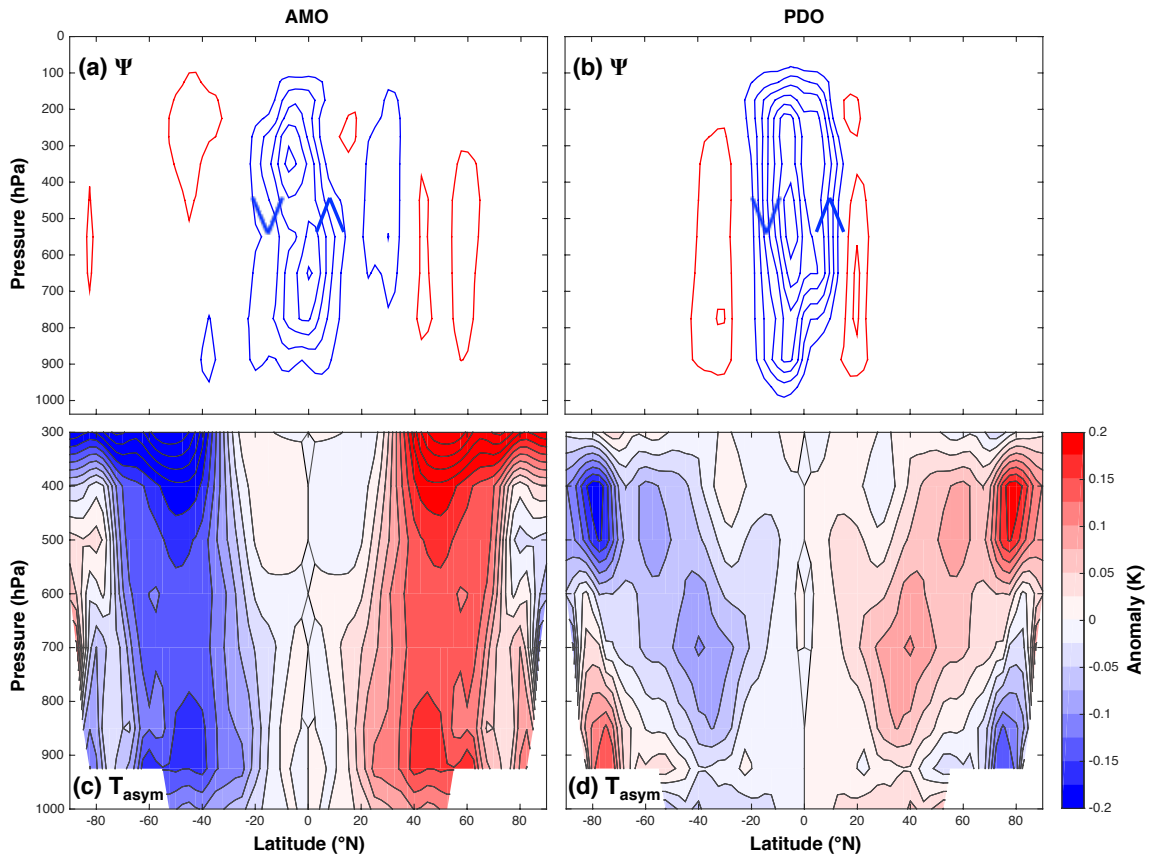
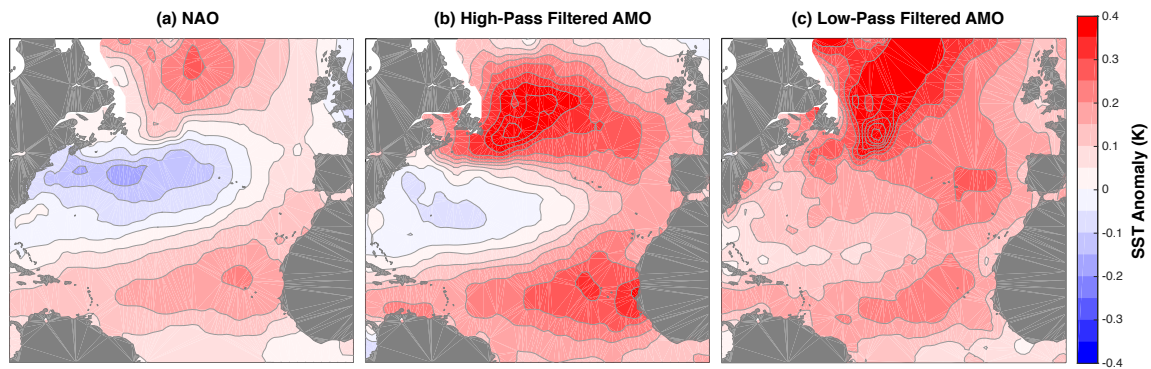


Table 1

		ITCZ	$\Psi_{eq}$	$T_{interhem}$
<b>AMO:</b>	<b>R<sup>2</sup></b>	0.11	0.41	0.74
	<b>Anomaly</b>	$0.07 \pm 0.05$ (°N)	$-2.9 \pm 1.1$ (Sv)	$0.17 \pm 0.05$ (K)
<b>PDO:</b>	<b>R<sup>2</sup></b>	0.14	0.17	0.02
	<b>Anomaly</b>	$0.10 \pm 0.06$ (°N)	$-3.3 \pm 1.7$ (Sv)	$0.04 \pm 0.07$ (K)

Supplementary Figure 1



Supplementary Figure 2

